Density of States of OLED Host Materials from Thermally Stimulated Luminescence

Andrei Stankevych,[1] Alexander Vakhnin,[1] Denis Andrienko,[2] Leanne Paterson,[2] Jan Genoe,[3] Ivan Fishchuk,[4] Heinz Bässler,[5] Anna Köhler,[5,6] and Andrey Kadashchuk[1,3,*]

[1] *Institute of Physics, Natl. Academy of Sciences of Ukraine, Prospect Nauky 46, 03028 Kyiv, Ukraine*
[2] *Max Planck Institute for Polymer Research, Ackermannweg 10, 5528 Mainz, Germany*
[3] *IMEC, Kapeldreef 75, 3001 Leuven, Belgium*
[4] *Institute for Nuclear Research, Natl. Academy of Sci. of Ukraine, Prospect Nauky 47, 03028 Kyiv, Ukraine*
[5] *Bayreuth Institute of Macromolecular Research (BIMF), Universitätsstr. 30, 95448 Bayreuth, Germany*
[6] *Soft Matter Optoelectronics and Bavarian Polymer Institute (BPS), Universitätsstr. 30, 95448 Bayreuth, Germany*

(Received 25 October 2020; revised 13 March 2021; accepted 2 April 2021; published 29 April 2021)

The electronic density of states (DOS) plays a central role in controlling the charge-carrier transport in amorphous organic semiconductors, while its accurate determination is still a challenging task. We apply the low-temperature fractional thermally stimulated luminescence (TSL) technique to determine the DOS of pristine amorphous films of organic light-emitting diode (OLED) host materials. The DOS width is determined for two series of hosts, namely, (i) carbazole-biphenyl derivatives, 4,4′-bis(*N*-carbazolyl)-1,1′-biphenyl (CBP), 3,3′-di(9*H*-carbazol-9-yl)-1,1′-biphenyl (mCBP), and 3′,5-di(9*H*-carbazol-9-yl)-[1,1′-biphenyl]-3-carbonitrile (mCBP-CN), and (ii) carbazole-phenyl (CP) derivatives, 1,3-bis(*N*-carbazolyl)benzene (mCP) and 9-[3-(9*H*-carbazol-9-yl)phenyl]-9*H*-carbazole-3-carbonitrile (mCP-CN). TSL originates from radiative recombination of charge carriers thermally released from the lower-energy part of the intrinsic DOS that causes charge trapping at very low temperatures. We find that the intrinsic DOS can be approximated by a Gaussian distribution, with a deep exponential tail accompanying this distribution in CBP and mCBP films. The DOS profile broadens with increasing molecular dipole moments, varying from 0 to 6 D, in a similar manner within each series, in line with the dipolar disorder model. The same molecular dipole moment, however, leads to a broader DOS of CP compared with CBP derivatives. Using computer simulations, we attribute the difference between the series to a smaller polarizability of cations in CP derivatives, leading to weaker screening of the electrostatic disorder by induction. These results demonstrate that the low-temperature TSL technique can be used as an efficient experimental tool for probing the DOS in small-molecule OLED materials.

DOI: 10.1103/PhysRevApplied.15.044050

I. INTRODUCTION

Determination of the electronic density of states (DOS) in disordered organic solids is of fundamental importance for the accurate physical understanding and modeling of charge-carrier transport in organic functional semiconductors and electronic devices. A Gaussian shape, $g(\varepsilon) \propto \exp[-1/2(\varepsilon/\sigma)^2]$, where σ is the width of the DOS, is a common approximation used for neat disordered organic solids [1–3], such as low-molecular-weight glasses and semiconducting polymers. Nondispersive photocurrent transients observed in amorphous organic materials [3] unambiguously support the notion of a Gaussian shape, rather than an exponential DOS [4,5]. The point is that, in the case of an exponential DOS, the time-of-flight (TOF) transients should always be dispersive because they would never equilibrate during the transit time at small carrier concentrations and should follow a dispersive transport model. The Gaussian DOS is also predicted by the central limit theorem, since the interaction energy of a charged molecule embedded in a random polarizable environment depends on a large number of neighboring neutral molecules [1,2].

Despite the success of the Gaussian disorder formalism, particularly for neat organic semiconductor films, the exact shape of the DOS can deviate from a Gaussian shape, for instance, in the far tail region of the DOS [6] or in doped organic films where the DOS is distorted by ionized dopants [7]. Consequently, charge-transport characteristics in sandwich-type diodes are often modeled by assuming that the DOS is a superposition of Gaussian and exponentially distributed trap states [8]. Recently, May *et al.*

*kadash@iop.kiev.ua

[9] showed that deep exponential tails could develop for molecules with large changes in molecular polarizability upon charging. Several direct experimental measurements of the DOS shape also demonstrate that the center of the DOS distribution is indeed Gaussian, but the tails can have a more complex structure [10,11].

The experimental determination of the DOS profile, however, is far from trivial. In contrast to inorganic semiconductors, the DOS of organic systems is not amenable to optical probing, because the direct optical transitions between the valence and conduction states are weak and masked by strong exciton transitions [12,13]. A number of experimental techniques are used to probe the DOS of organic films, such as temperature-dependent space-charge-limited-current spectroscopy [14], ultraviolet photoelectron spectroscopy (UPS) [15], inverse photoemission spectroscopy (IPS) [16], Kelvin probe force microscopy (KPFM) [10,11], the electrochemically gated transistor approach [17], as well as thermally stimulated luminescence (TSL) [18]. A clear advantage of TSL is that it is a purely optical and electrode-free technique. This helps to eliminate interface or contact effects, and it allows DOS measurements in materials with low charge-carrier mobilities and in systems with large energy disorder where charge transport is very dispersive.

TSL is the phenomenon of luminescent emission after removal of excitation (UV light in our case) under conditions of increasing temperature. First, photogenerated charge carriers populate trap states, usually at very low temperatures. Once the sample is heated, typically with a linear temperature ramp, trapped charge carriers are released and then recombine, producing luminescence emission. Technically, TSL is a relatively simple technique with straightforward data analysis. However, it should be noted that the mechanism of TSL in amorphous organic semiconductors with a broad energy distribution of strongly localized states differs from the mechanism commonly accepted for crystalline materials with band-type transport, where a discrete trapping-level model is applicable. A specific feature of amorphous solids is that localized states within the lower energy part of the intrinsic DOS distribution can give rise to shallow charge trapping at very low temperatures, and, as a consequence, TSL can be observed even in materials where the "trap-free limit" is postulated. Since TSL measurements are normally performed after a long dwell time after photoexcitation, the initial energy distribution of localized carriers is formed after low-temperature energy relaxation of photogenerated carriers within a Gaussian distribution of DOS and, therefore, the first thermally assisted jumps of relaxed carriers are considered as the rate-limiting steps determining TSL. This is in contrast to thermally stimulated conductivity, which is believed to be governed by the interplay between trapping and detrapping processes [4]. The theoretical background for the application of TSL for probing the DOS distribution in disordered organic systems has been developed [18,19] using a variable-range hopping formalism and the concept of thermally stimulated carrier random walk within a positionally and energetically random system of hopping sites. The theory proves that the high-temperature wing of the TSL curve in such amorphous materials should be an exact replica of the deeper portion of the DOS distribution [18,19] and yields the effective DOS width.

TSL is particularly suitable for probing the DOS and extrinsic traps in luminescent organic materials, such as π- and σ-conjugated polymers [18,20–26], molecularly doped polymers [27,28], oligomers [29], and hybrid organic-inorganic perovskite films [30]. Here, we use TSL to characterize the DOS in spin-coated films of two series of organic semiconducting materials of different polarity, based on small-molecule carbazole-biphenyl (CBP) derivatives, CBP, mCBP, and mCBP-CN (series 1), and carbazole-phenyl (CP) derivatives, mCP and mCP-CN (series 2), the chemical structures of which are shown in Fig. 1. These materials are widely used as hosts for blue triplet emitters or for emitters based on thermally activated delayed fluorescence (TADF) in organic light-emitting diodes (OLEDs), due to their wide band gaps and high triplet energies. They are also used as charge-transporting layers in both OLED and hybrid perovskite-based light-emitting devices. A suitable polarity of these materials is important for optimizing the performance of TADF-based OLED devices.

In our study, the TSL data are analyzed using the Gaussian disorder formalism, based on a thermal release of charge carriers from the lower-energy part of the intrinsic DOS distribution. We find that, for materials with similar core chemical structures, the DOS broadens with increasing dipole moment, in essentially the same manner for both series of CBP and CP derivatives, in agreement with the dipolar disorder model. Systematic differences in the DOS widths are observed between these two different series of derivatives. This is attributed to different nonpolar contributions to the DOS of these materials, which are analyzed using a theoretical approach based on the distributed electrostatic model. Large DOS widths are found in strongly polar hosts, and good agreement between experimental and computational results proves the intrinsic character of the large energy disorder in these materials. TSL measurements also show that the Gaussian-shaped DOS of CBP and mCBP are both accompanied by a deep exponential tail.

II. EXPERIMENT

A. Materials

CBP, mCBP, mCBP-CN, mCP, and mCP-CN are purchased from Lumtec Corp. and used as received. Thin films of the above compounds are spin-coated from

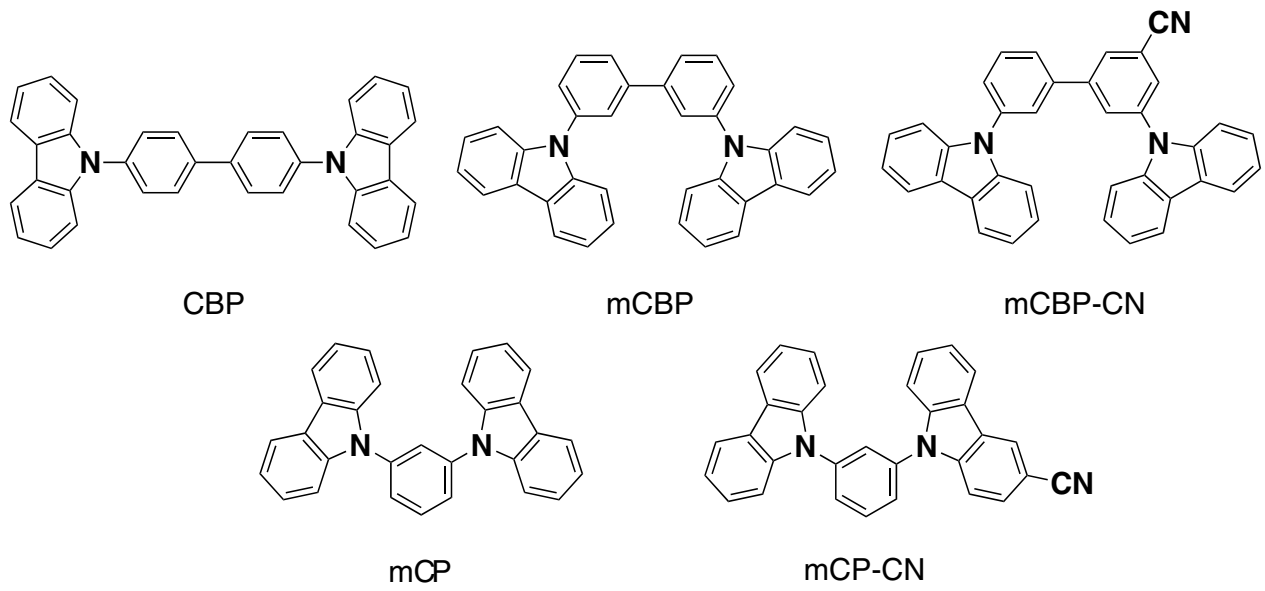

FIG. 1. Molecular structures of compounds used in this study. CBP derivatives, 4,4′-bis(*N*-carbazolyl)-1,1′-biphenyl (CBP); 3,3′-di(9*H*-carbazol-9-yl)-1,1′-biphenyl (mCBP); and 3′,5-di(9*H*-carbazol-9-yl)-[1,1′-biphenyl]-3-carbonitrile (mCBP-CN). CP derivatives, 1,3-bis(*N*-carbazolyl)benzene (mCP) and 9-[3-(9*H*-carbazol-9-yl)phenyl]-9*H*-carbazole-3-carbonitrile (mCP-CN).

20 mg/ml chloroform solutions onto cleaned quartz substrates (1000 rpm, 30 s) that result in typically 150-nm-thick layers. Subsequently, the deposited films are dried in an oven at 40 °C for 10 m and then under vacuum for 2 h to remove residual solvent.

B. TSL technique

TSL measurements are carried out over a temperature range from 4.2 to 300 K with an accuracy better than 0.1 K using an optical temperature-regulating liquid-helium bath cryostat designed and fabricated by the Cryogenic Technologies Laboratory [77] at the Institute of Physics of National Academy of Sciences of Ukraine. In this type of cryostat, the sample is attached to the end of a sample manipulator and is suspended in a helium heat-transfer gas environment inside the inner sample chamber. The sample temperature is controlled by the temperature controller unit in a twofold manner: (i) via two separate heating elements (one is integrated into the sample holder, directly heating the sample, and the second one is mounted in the sample chamber, heating the heat-transfer gas), and (ii) by regulating the helium flow between the helium bath and the sample chamber via control of the He gas pressure in the sample chamber.

In TSL experiment, samples are cooled to 4.2 K and irradiated for 30 s with $\lambda_{exc} = 313$ nm light (cw excitation, light power density is about 5 mW/cm^2) selected by appropriate set of cutoff filters from a high-pressure 250 W Hg lamp. No sample heating occurs during UV-light illumination and the sample is immersed in liquid helium. The studied organic films do not exhibit any notable photodegradation during the measurements. TSL measurements are done as follows: first, after terminating photoexcitation, the samples are kept in the dark at a constant temperature, $T = 4.2$ K, during a certain dwell time (typically for 10 min) to allow all isothermal emission processes, like phosphoresce and isothermal recombination of short-range geminate charge-carrier pairs, to decay to a negligible level. Then TSL is detected upon heating the sample, and TSL emission is detected in photon-counting mode with a cooled photomultiplier positioned next to the cryostat window.

TSL measurements are performed in two different regimes: uniform heating at a constant heating rate β of 0.15 K/s and under the fractional heating regime. Details of the TSL measurements are described elsewhere [21,22,27]. The method of fractional TSL avoids the disadvantages of common glow curve methods based on the constant heating rate – it is characterized by greater accuracy and a high resolving power, and it does not require knowledge of the frequency factors and retrapping probabilities [31,32]. The low-temperature fractional TSL is extensively applied by our group to investigate charge-carrier trapping in a great variety of organic semiconductor materials. The fractional heating TSL technique (also called the fractional glow technique), originally proposed by Gobrecht and Hofmann [32] is an extension of the initial rise method and is based on cycling the sample with a large number of small temperature oscillations superimposed on a uniform heating ramp. The main reason for applying this method is that the usual quantitative evaluation of the

TSL glow curves is very inaccurate, or even impossible, if the traps are continuously distributed in energy or if there are several types of traps with discrete but very close lying activation energies. In this case, the glow peaks fuse together, and individual glow maxima may not be discernible. The mean activation energy, E, is determined during each temperature cycle with a temperature change, ΔT, as

$$E(T) = -\frac{d[\ln I(T)]}{d(1/kT)};\ \text{at}\ \beta = \text{const},\ \Delta T \ll T,\ n \ll n_{\text{tot}} \tag{1}$$

where $I(T)$ is the intensity of the TSL, T is the temperature, and k is the Boltzmann constant. Here, n is the number of charge carriers released during each temperature cycle, and n_{tot} is the total number of carriers trapped by the same sort of traps. These conditions determine the so-called "initial rise method," which is actually the basis for Eq. (1). Since a temperature oscillation, ΔT, is usually much less than the mean value of T, E can be assumed to equal $E(T)$, the activation energy of traps emptied at temperature T. A trap distribution function, $H(E)$, can be determined in arbitrary units as [31–33]

$$H(E) \propto \frac{I(E)}{dE/dT}, \tag{2}$$

where $I(E\ )$ is TSL after converting the temperature scale to the energy scale by means of empirically accessible $E(T)$ dependence obtained by Eq. (1). As one can see from Eq. (2), in the case when $E(T)$ is a linear function, the TSL intensity dependence, $I(T)$, is an exact replica of the populated trap distribution function [19]. The frequency factor at the maximum of TSL peak, S, is given by

$$S = E_m\beta/kT_m^2 exp\,(E_m/kT_m) \tag{3}$$

where T_m and E_m are the temperature and activation energy of the maximum of the TSL peak, respectively. All measurements are done under a helium atmosphere.

C. Computer simulations

For morphology simulations, we adapt the all-atom optimized potentials for liquid simulations (OPLS-AA) force field [34–36]. All Lennard-Jones parameters are taken from this force field and we use the OPLS combination rules and the fudge factor of 0.5 for 1–4 interactions. Atomic partial charges are computed via the charges from electrostatic potentials using a Grid-based method (CHELPG) scheme [37]. We partition the molecules into rigid fragments: carbazoles and bridge groups in between. These rigid fragments are orientated with respect to one another, such that conformers exhibit different energies, as a result of different electrostatic interactions. The dihedral interaction potentials that connect these fragments are parameterized as described elsewhere [38]: for each fixed value of the dihedral angle, the geometry is optimized at the m06-2x/6-311g(d,p) level. The potential difference is then fitted to the Ryckaert-Belleman polynomial, $V_{\text{RB}}(\theta) = \sum_{n=0}^{5} (\cos\,\theta\ )^n$.

The long-range electrostatic interactions are treated by using the smooth-particle-mesh Ewald technique. A cutoff of 1.3 nm is used for the nonbonded interactions. The equations of motion are integrated with a time step of 0.002 ps. All molecular dynamics (MD) simulations are performed in the *NPT* ensemble using the canonical velocity-rescaling thermostat [39] and the Berendsen barostat [40], as implemented in the GROMACS simulation package [41,42].

To obtain the *amorphous* morphology, 3000 molecules are prearranged on a lattice and compressed (anisotropic *NPT* barostat) at $T = 800$ K for 1 ns. The system is then cooled to 300 K during a 1 ns run. Fast cooling freezes the isotropic orientation of the high-temperature liquid, leading to amorphous molecular ordering.

Using the molecular dynamics trajectories, we evaluate the anion, cation, and neutral-state energies for each molecule in a morphology using a perturbative approach [43–45]. In this approach, the total energy is a sum of the gas-phase, electrostatic, and induction contributions, $E_{e,h,n} = E^{\text{gas}}_{e,h,n} + E^{\text{stat}}_{e,h,n} + E^{\text{ind}}_{e,h,n}$. To evaluate the electrostatic contribution, we use distributed atomic multipoles up to the fourth order. The induction contributions to site energies are calculated self-consistently using the Thole mode [46,47] on the basis of the atomic polarizabilities and distributed multipoles obtained by using the GDMA program [48] for a cation, anion, and a neutral molecule. All calculations are performed using the aperiodic Ewald summation scheme [45], as implemented in the in-house-developed VOTCA package [49].

III. RESULTS

A. DOS probing by TSL measurements

Surprisingly, strong thermoluminescence signals induced by UV radiation at liquid-helium temperature are observed in neat thin films made of both CBP and CP derivatives studied in the present work. First, we consider TSL measurements in thin films of CBP derivatives. A typical TSL glow curve of a mCBP-CN film measured after photoexcitation with 313 nm at 4.2 K is presented in Fig. 2(a) and it reveals a broad slightly asymmetric band, with the maximum at $T_m \cong 93$ K. The asymmetric shape of the TSL band might be due to overlapping of the main high-temperature peak at 93 K, with a weaker low-temperature peak at around 40 K, as depicted by curves $1'$ and $1''$ in Fig. 2(a). The TSL signal is observed immediately upon heating the sample and extends to about

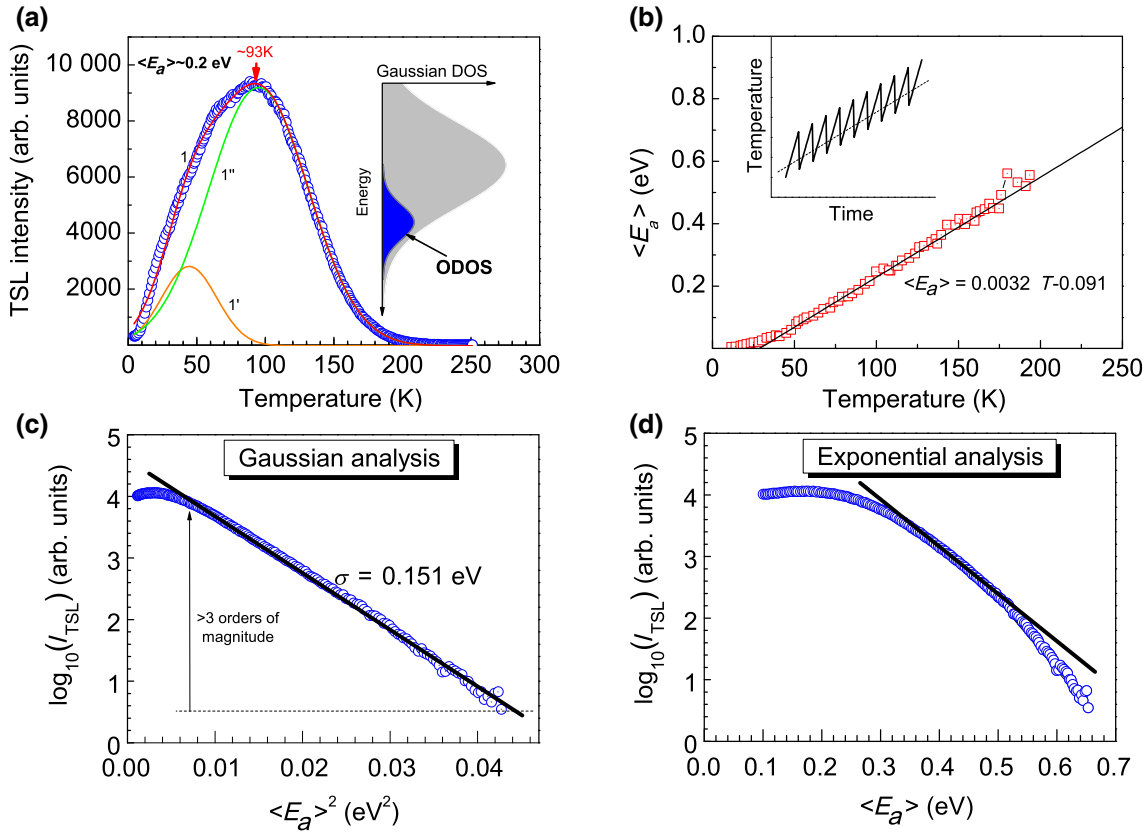

FIG. 2. (a) Spectrally integrated TSL glow curve measured after excitation with 313 nm light for 3 min at 4.2 K for mCBP-CN film. Curves 1′ and 1″ represent deconvolution of the TSL band (curve 1) into two Gaussians. Inset shows schematic DOS distribution together with the distribution of trapped charge carriers at liquid-helium temperature after energy relaxation. (b) Temperature dependence of the mean activation energy $\langle E_a \rangle$ as obtained by fractional TSL (symbols) and extrapolation by an empirical expression, Eq. (4) (solid line). Inset shows schematic picture to illustrate principle of fractional TSL regime, when temperature oscillations are superimposed on uniform heating. (c) Gaussian analysis of the high-energy part of the TSL curve. (d) Same data as in (c) but plotted in exponential representation.

220 K, as expected for a disordered material devoid of deep charge-carrier traps. It is qualitatively similar to TSL phenomena observed in other organic disordered systems studied before [18–23] and can be ascribed to detrapping of charge carriers from the localized states that occupy the lower-energy part of the intrinsic DOS distribution, as schematically shown in the inset of Fig. 2(a). The fact that TSL in mCBP-CN films extends to moderately high temperatures is evidence of relatively strong energy disorder in this material, compared, for instance, with conventional semiconducting polymers, such as a methyl-substituted ladder-type poly(*para*-phenylene) [18] and a polyfluorene derivative [20] with reduced energy disorder. Yet, it is closer to the TSL peak observed before in TSL of vacuum-deposited films of AlQ_3 [50].

Similar to previously studied photoconducting polymers [18–22,27], the mCBP-CN film is characterized by a quasicontinuous trap distribution, with a mean activation energy, E_a, that is linearly increasing with temperature [Fig. 2(b)], as revealed by fractional TSL measurements (see the Experiment Section II B for details). The temperature dependence of E_a (in eV) can be described by the following empirical relation:

$$E_a(T) = 0.0032T - 0.091. \tag{4}$$

The empirical expression given by Eq. (4) supports the basic formula of Simmons-Taylor theory [51] for a thermally stimulated current (TSC), which predicts a qualitatively similar linear temperature dependence of the apparent activation energy. It is worth noting that such kinds of linear relationship for $E_a(T)$ are also justified by analytically variable range-hopping calculations for disordered organic semiconductors [18,19]. The mean activation energy and frequency-to-escape factor at the maxima of the TSL peak, $T_m \sim 93$ K, are $E_a \cong 0.2$ eV and $\langle S \rangle = 2.7 \times 10^9$ s^{-1}, respectively. The meaning of the frequency-to-escape factor in disordered solids will be discussed in more detail in Sec. IV B.

TABLE I. Dipole moment (p), polarizability of a neutral molecule ($\alpha_{neutr.}$), polarizability of a cation ($\alpha_{cation.}$), and width of the Gaussian DOS (σ) evaluated by TSL and computer simulations; dipolar disorder component (σ_{dip}) estimated from TSL data; and width of superimposed exponential low-energy tail (T_0) evaluated from TSL data.

Material	Dipole moment, p (D)	$\alpha_{neutr.}$(Bohr^3)	α_{cation}(Bohr^3)	DOS width (TSL) σ (eV)	σ_{dip}(eV)	T_0, (K)	DOS width (simulations) σ (eV)
CBP	0.04[a]	670[b]	3200[b]	0.125	0	716	0.10
mCBP	2.15[a]	600[b]	3000[b]	0.131	0.039	673	0.12
mCBP-CN	4.6[a]	600[b]	3000[b]	0.151	0.085	–	0.20
mCP	1.35[a]	450[b]	1500[b]	0.140	0.024	–	0.16
mCP-CN	6[a]	540[b]	1500[b]	0.177	0.111	–	0.24

[a]Calculated by using the M062X functional in density-functional theory.
[b]Calculated using a perturbative approach, as implemented in the Gaussian 09 package (opt = polar) keyword [78].

Using an empirical calibration of Eq. (4) to convert the temperature scale to a trap-energy scale, and then plotting the high-temperature part of the TSL signal intensity logarithmically either against E_a^2 or E_a, allows for a "Gaussian" or an "Exponential analysis," respectively, as shown in Figs. 2(c) and 2(d). It proves that the high-temperature part of a TSL curve becomes a straight line when plotting $\ln(I_{TSL})$ versus E_a^2 [Fig. 2(c)]. It is remarkable to see an almost perfect Gaussian fit of the high-temperature part of the measured curve observed over three decades of TSL intensity variation [Fig. 2(c)], whereas the same data plotted in the $\log(I_{TSL})$ versus E_a representation show a clear deviation from an exponential dependence [Fig. 2(d)]. This observation provides strong support for a Gaussian shape of the DOS profile in this material. The slope of the straight line in Fig. 2(c) is a measure of the DOS width. The energy disorder parameter $\sigma = 0.151$ eV is obtained for the mCBP-CN film, which is very close to the disorder parameter $\sigma = 0.15$ eV estimated for AlQ_3 films [52] by charge-transport measurements. Such a relatively strong energy disorder is expected for polar materials – the dipole moments for AlQ_3 [52] and mCBP-CN are 4.9 and 4.6 D, respectively (Table I). It is worth noting that the above Gaussian analysis used here is conceptually similar to that earlier employed by Bässler [53] and Eiermann *et al.* [54] using the TSC technique for studying the width of the DOS distribution in disordered tetracene layers, by analyzing the shape of the high-energy part of a TSC peak.

Figure 3(a) compares normalized TSL curves measured for CBP, mCBP, and mCBP-CN films under the same conditions. All of these host materials reveal a characteristic TSL peak, which features a clear shift and progressive broadening towards higher temperatures with increasing molecular dipole moment [Fig. 3(a)]. The TSL peak maximum [depicted by arrows in Fig. 3(a)] also shifts from $T_m \cong 72$ K for CBP to $T_m \cong 78$ and 93 K for mCBP and mCBP-CN films, respectively (Table I). The latter effect is a clear sign of increasing energy disorder

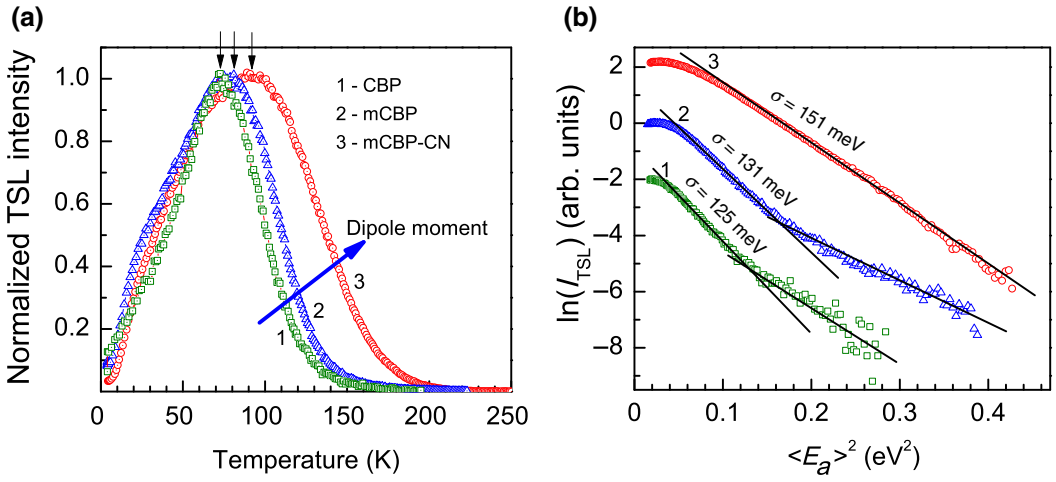

FIG. 3. (a) Normalized TSL glow curves measured after excitation with 313 nm light for 3 min at 4.2 K for CBP, mCBP, and mCBP-CN films (curves 1, 2, and 3, respectively); (b) Gaussian analysis of high-temperature parts of TSL curves shown in (a). Curves are vertically shifted with respect to each other for clarity.

in this sequence of host materials from the same series of CBP derivatives. The shift is a consequence of the fact that the mean activation energy, which carriers reach in the course of their downward hopping relaxation at very low temperature within a Gaussian DOS, is directly proportional to energy-disorder parameter σ [55].

A Gaussian analysis of the high-temperature parts of TSL curves for CBP, mCBP, and mCBP-CN films, using Eq. (4), as described above, is shown in Fig. 3(b). The plot reveals a Gaussian dependence in all samples—its slope yields the width of the DOS, which increases with increasing dipole moment from 0.125 eV for virtually nonpolar CBP ($p \cong 0$ D) to 0.131 and 0.151 eV for mCBP ($p = 2.15$ D) and mCBP-CN ($p = 4.6$ D), respectively (cf. Table I). This points to an important role of the dipolar-disorder effects on the increase of the energy disorder in this series of CBP derivatives, with increasing dipole moments of constituent molecules. The disorder parameter $\sigma = 0.112$ eV [56] is inferred for evaporated CBP films from charge-transport measurements, which is comparable to the value of $\sigma = 0.125$ eV we obtain here for the spin-coated CBP film.

A remarkable observation of this study is that CBP and mCBP films also reveal slower-decaying deep exponential tails at the lowest portion of the DOS, following the Gaussian distribution. Fitting the deep tail with exponential distribution $g(\varepsilon) \propto \exp(\varepsilon/kT_0)$, where T_0 is the characteristic width of the exponential distribution (for energies $\varepsilon < 0$), yields 716 and 673 K, for CBP and mCBP films, respectively (Table I).

Next, we compare the TSL properties of the above CBP derivatives with another series of host materials, based on CP derivatives. TSL glow curves measured under the same conditions for mCP and mCP-CN films are shown in Fig. 4(a) (curves 1 and 2, respectively). Although these films exhibit a TSL signal within a similar temperature range, from 4.2 to about 200 K, to that of the CBP derivatives [cf. Fig. 3(a)], the shapes of their TSL curves are significantly different. The TSL curve of mCP clearly consists of two overlapping peaks with T_m at 25 and 65 K, respectively, as shown by deconvolution of the measured TSL curve into two Gaussian peaks (curves 1′ and 1″ in Fig. 4). It is noteworthy that the low-temperature feature with $T_m = 25$ K dominates in intensity. A similarly shaped TSL is found in the strongly polar mCP-CN film ($p = 6$ D) [Fig. 4(a), curve 2], which also consists of two overlapping peaks, but are shifted towards higher temperatures with T_m at 33 and 78 K. We should, however, note that a low-temperature feature is also noticeable in TSL curves of mCBP and mCBP-CN films, but it is significantly weaker and seen as just a weak shoulder [cf. curve 1′ in Fig. 2(a)]. Our complementary studies demonstrate that the low-temperature TSL feature in these materials arises due to frustrated energy relaxation [57] of charge carriers photogenerated at 5 K, and therefore, some of them get stuck in the upper portion of the DOS; this effect will be explored in greater detail in future works of the authors. Since only the deeper portion of the DOS profile controls charge transport in amorphous organic semiconductors, the high-temperature TSL feature, peaking at 65 and 78 K in mCP and mCP-CN, respectively, is expected to be of practical relevance (we refer to it as the "main TSL peak"), and thus, is analyzed below.

The mean activation energy E_a is measured in mCP and mCP-CN films as a function of temperature by fractional TSL and in both materials it exhibits a similar temperature dependence to that given by Eq. (4). Gaussian analysis of the high-temperature parts of TSL curves for mCP and mCP-CN films is done as described above for other host materials and is presented in Fig. 4(b) as curves 1 and 2,

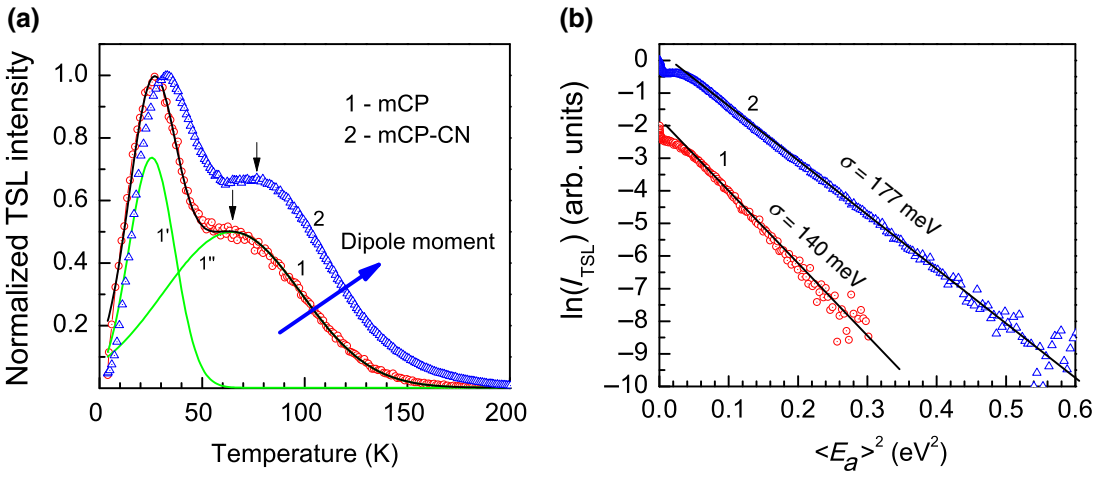

FIG. 4. (a) Normalized TSL glow curve measured after excitation with 313 nm light for 3 min at 4.2 K for mCB and mCP-CN films (curves 1 and 2, respectively). Curves 1′ and 1″ represent deconvolution of the TSL curve of mCP (curve 1) into two Gaussian peaks; (b) Gaussian analysis of high-temperature part of the corresponding TSL curves shown in (a).

respectively. The energy-disorder parameter, σ, in these materials is inferred from the slope of the high-temperature part of TSL curves plotted in a Gaussian representation: $\ln(I_{TSL})$ versus ${E_a}^2$. Both materials show a nice Gaussian fitting of the high-temperature parts of the measured curves over several decades of TSL intensity variation. Since the TSL signal in the mCP-CN film is significantly stronger than that in mCP, we are able to extend its Gaussian analysis towards deeper energies [Fig. 4(b), curve 2]. The results in Fig. 4(b) demonstrate a clear impact of the magnitude of the dipole moments on the width of the DOS, which increases from $\sigma = 0.140$ eV for moderately polar mCB ($p = 1.35$ D) to 0.177 eV in strongly polar mCP-CN ($p = 6$ D). This suggests a rather significant energy disorder that is inherent in CB derivatives.

B. Computation of the DOS distribution

To provide deeper insights into the DOS structure and independent verification of the DOS parameters probed by the TSL technique in the above OLED host materials, we carry out computer simulations. To evaluate the DOS distribution of the amorphous systems, we initially employ atomistic MD simulations to generate the amorphous morphologies, as described in Sec. II C. We then use quantum chemical calculations and polarizable force fields to compute site energies. Using the simulated amorphous morphologies, site energies of all molecules are evaluated by using the parameterized (see the Sec. II C) polarizable force fields. The corresponding DOS, shown in Fig. 5, have Gaussian shapes with variances σ.

The DOS widths σ inferred from the simulation results are listed in Table I. Despite the similarity in chemical structures of CBP derivatives, the energy disorder varies over a broad range in these materials from 0.10 eV to 0.12 and 0.20 eV for CBP, mCBP, and mCBP-CN, respectively.

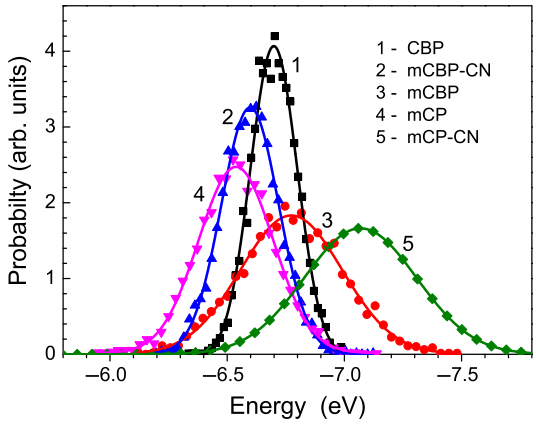

FIG. 5. DOS distributions calculated for CBP, mCBP, mCBP-CN, and mCP (curves 1, 2, 3, and 4, respectively) employing molecular dynamics simulations. Solid lines depict Gaussian fits to data.

As expected, the smallest energy disorder is found in CBP films and this can be readily explained by the symmetric molecular structure: its ground-state dipole moment is virtually zero. As a result, the first nonvanishing electrostatic contribution is due to the interaction of the charge carrier and the quadrupole moments of the surrounding molecules. Since this contribution is much smaller than the charge-dipole interaction, the energetic disorder of these compounds is relatively small, in the order of 0.1 eV. The shift of the ionization potential in a solid state is mostly due to induction stabilization, and the shape of the density of states is Gaussian. The dipole moment increases sequentially in mCBP and mCBP-CN molecules, which gives rise to the increase of charge-dipole integration and hence to a larger electrostatic contribution to the energetic disorder in these materials. This verifies that dipolar disorder is responsible for the significant increase in the energy disorder within the series of CBP derivatives. Such a conclusion is, however, valid for compounds of the same family, in our case, with similar molecular polarizabilities. Indeed, the DOS simulations confirm that the CBP, mCBP, and mCBP-CN family has similar polarizability of cations and neutral molecules (see Table I), and hence, their DOS width increases with the molecular dipole moment. mCP has a significantly smaller polarizability of the cation compared with mCBP (∼1500 vs ∼3000 Bohr^3, see Table I). Therefore, screening of the electrostatic disorder by the induction interactions is smaller than that for mCBP, giving rise to a DOS width of 0.16 eV for mCP.

It is pertinent to note that dipole moments can vary considerably with molecular conformations. Different conformers lead to variations in the molecular dipole

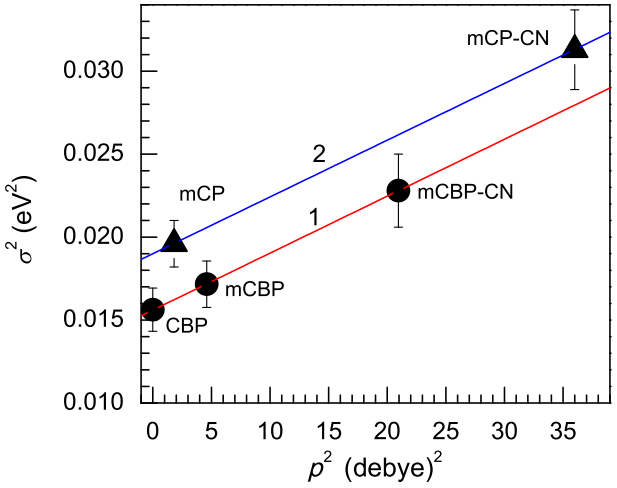

FIG. 6. Estimated disorder parameter versus dipole moment for two series of OLED host materials: CBP and CP derivatives (solid circles and triangles, respectively). Solid lines are results of fitting of experimental data with Eqs. (5) and (6) using $c = 1$ and $\varepsilon = 3.13$ [71].

moment in the amorphous morphologies. The distribution of dipole moments in the morphology inferred from MD simulations normally features a fairly broad peak [75] around a certain value that can, to a certain extent, be used as the "average" dipole moment. We are not claiming that this trend is universal for all organic semiconductors, especially taking into account that the distributions of dihedral angles are sensitive to the deposition protocols. However, in our host materials, the average dipole moments inferred from MD simulations [75] are found to correlate well with those shown in Table I and are used for the analysis depicted in Fig. 6.

IV. DISCUSSION

The DOS widths determined by the TSL techniques are in reasonable agreement with the computation results (cf. Table I), predicting a significant variation in energy disorder among the considered host materials. Although the obtained experimental values somewhat deviate from the simulated σ values, mostly in systems with strong energy disorder, they do demonstrate a remarkably *similar trend* in the variation of energetic disorder among these materials. The reason for the discrepancy between the widths of the DOS probed by TSL and that obtained by computer simulations should be a subject of further research.

A comparison of the DOS parameters determined by TSL and by computer simulations (Fig. 5) has two important implications: (i) It confirms that the large energetic disorder observed experimentally (ranging from $\sigma = 0.125$ to 0.177 eV) characterizes the *intrinsic* DOS, i.e., the DOS of a chemically pure disordered material, rather than that affected by impurity-related traps. Therefore, charge transport in such OLED hosts is expected to be inherently very dispersive. (ii) It reveals the utmost importance of the polarizability of the cation for the DOS width, which is a key finding in the present study. As attested by computer simulations, the physical reason for the enlarged energetic disorder in CP derivatives compared with CBP ones can be attributed to much smaller polarizability of their cation states, owing to the more rigid chemical structure of these molecules, and thus, smaller screening effect.

The calculated DOS distributions in Fig. 5 yield not only the variances, σ, of their Gaussian shapes, but also the energy positions of the HOMO levels. On the other hand, methods based on thermally activated spectroscopy, like TSL or TSC, use thermal energy generated by heat to probe localized states occupied by charge carriers within intrinsic (or extrinsic) DOS. Since such an energy is much less than that of the energy corresponding to the HOMO-LUMO gap, it can only characterize the DOS parameters. Nonetheless, in host-guest compositions, TSL can potentially yield the energy difference between corresponding HOMO or LUMO levels of host and guest materials, if guest molecules create a hole or an electron trap, respectively, in the host material.

A. Effect of dipole moments

Next, we discuss the effect of the dipole moments, of the materials studied here, on the width of the DOS evaluated by the TSL technique. As it has long been suggested, the total width σ in a polar amorphous organic solid can be decomposed into a dipolar component, σ_{dip}, and a so-called van der Waals component, σ_{vdW} [3,58]. If different energy-disorder contributions are independent and follow Gaussian statistics, then the total width is

$$\sigma^2 = \sigma_{\mathrm{vdW}}^2 + \sigma_{\mathrm{dip}}^2. \tag{5}$$

The term σ_{vdW} in Eq. (5) is used here to describe the whole nondipolar disorder component, despite its physical origin being solely attributed to the variation of the interaction of a charged molecule with induced dipole moments in the molecular environment [59,60]. Borsenberger and Weiss [3] proposed that fluctuations of relative orientations and intermolecular distances between the hopping site and surrounding molecules created fluctuations of the induced dipolar cloud in nearby molecules, which made the major contribution to σ_{vdW}. Subsequently, it is recognized that quadrupole moments can be sufficiently high in nonpolar materials with zero dipole moment, and hence, variation of charge-quadrupole interactions can also contribute to the energy disorder [9,61]. Therefore, to adhere to established terminology, we imply here that σ_{vdW} encompasses contributions from all sources of energy disorder, excluding the dipolar contribution. In other words, it describes the total energy disorder in a nonpolar system.

The dipolar disorder, σ_{dip}, contributes strongly to the overall energy disorder in polar organic solids, and it leads to a stronger DOS broadening compared with the charge-quadrupole interaction [61]. σ_{dip} arises due to randomly oriented permanent molecular dipoles that generate fluctuation in the electrostatic potential due to charge-dipole interactions, in addition to the disorder that is already present in nonpolar systems, which leads to DOS broadening [3]. Dieckmann *et al.* [58] originally obtained an expression for the dipolar component using Monte-Carlo numerical calculations. Subsequent analytical calculation by Young [62] has confirmed the Gaussian form of the DOS in polar systems and the relation for σ_{dip} is derived as

$$\sigma_{\mathrm{dip}} = \frac{7.04}{a^2\varepsilon} c^{1/2} p \ \text{(in eV)} \tag{6}$$

where a is the intersite distance (lattice constant) in Angstrom, ε is the dielectric constant, c is the fraction of the lattice occupied by dipoles (in our case $c = 1$), and p is the dipole moment in debye. Although, as recently

recognized [63], accounting for the individual molecular polarizabilities and nearest-neighbor interactions might lead to deviation from the suggested $1/\varepsilon$ dependence in Eq. (6), the dipolar disorder σ_{dip} is predicted to scale linearly with dipole moment. An analysis based on Eq. (6), in conjunction with Eq. (1), is widely used to evaluate the dipolar-disorder contribution to the overall energy disorder from charge-transport measurements in small-molecule organic glasses [3,64–66] and molecularly doped polymers, [3,60,67–69] with different dipole moments and dipole concentration, which justifies the applicability of Eq. (6).

Assuming the σ_{vdW} component is a constant for materials within the same series of derivatives, Eqs. (2) and (3) provide a means for analyzing the effect of the dipole moments of different compounds on the total width, by plotting σ^2 versus p^2. Figure 6 (curve 1) clearly shows the predicted linear relationship for the CPB derivatives, CBP, mCBP, and mCBP-CN (solid circles), indicating the justification for the analysis. The nonpolar component σ_{vdW} for this series of derivatives is equal to the DOS width, $\sigma = 0.125$ eV, obtained for a nonpolar CBP film. Using $\sigma_{\mathrm{vdW}} = 0.125$ eV, Eq. (5) yields the dipolar component $\sigma_{\mathrm{dip}} = 0.039$ and 0.085 meV, for polar mCBP and mCBP-CN, respectively (Table I). The intersite distance, $a = 11$ Å, may be estimated from the slope of solid line 1 in Fig. 6 using Eq. (6). It agrees well with the effective lattice constant $a = 12$ Å estimated recently for CBP films from charge-transport measurements [70].

A qualitatively similar trend with increasing dipole moment is found for a series of CP derivatives (Fig. 6, curve 2), although only two host materials (mCP and mCP-CN) of this series are available to us. The energy-disorder parameter demonstrates a strong increase with increasing dipole moment from 1.35 to 6 D for mCP and mCP-CN, respectively (Fig. 6, solid triangles). It is remarkable that this dependence in the σ^2 versus p^2 representation features almost the same slope (curves 2 in Fig. 6) as that of the linear dependence obtained for the above CBP derivatives (curve 1), but is offset with respect to the latter. These observations suggest that the dipolar-disorder component increases in a similar manner with increasing dipole moments for both series of materials, while the nonpolar σ_{vdW} disorder component differs significantly for them. The value of $\sigma_{\mathrm{vdW}} = 0.138$ eV is determined for mCP and mCP-CN from the $p^2 = 0$ intercept of curve 2 (Fig. 6), which turns out to be significantly larger than the value of $\sigma_{\mathrm{vdW}} = 0.125$ eV determined for the above series of CBP derivatives. Using the above σ_{vdW} value, Eq. (5) yields $\sigma_{\mathrm{dip}} = 0.024$ and 0.111 meV, for mCB and mCB-CN films, respectively (Table I). The above findings suggest that the enlarged energy disorder in CP, compared with CBP, derivatives, mostly relates to the intrinsically larger nondipolar component of energy disorder.

The correlation of the observed dipole effect on DOS width, as determined by the TSL technique, with the prediction of the dipolar disorder model [62], is striking. It implies that the OLED host materials considered here behave similarly to conventional amorphous organic photoconductors, as previously studied by the TOF technique in the form of neat molecular glasses [3,64–66] or as charge-transporting molecules in molecularly doped polymers [3,60,67–69]. It should be noted that the dipolar-disorder model given by Eq. (6) does not consider variations in the molecular dipole moment caused by different conformers in the amorphous morphologies. However, despite the simplification, we believe that this model can provide a good first-order approximation for a description of the dipolar-induced DOS broadening in our OLED hosts. Notably, the dependence presented in Fig. 6 and concomitant analysis is generally not a surprising result for the class of organic semiconducting materials. There are numerous similar findings in the literature for the width of the DOS inferred from charge-mobility measurements in different polar systems. The key result of the present work is that the same effects are observed using a purely optical experimental approach.

Finally, it worth mentioning that Hoffmann *et al.* [76] have recently demonstrated that, in contrast to small-molecule organic materials, the inhomogeneous broadening of the DOS for holes and neutral excitons can be remarkably similar in the case of conjugated polymers. This is suggested to be a characteristic feature of conjugated polymers, in which disorder results predominantly from the statistical variation of the lengths of the conjugated segments, rather than from van der Waals coupling among the chains and can be used for the prediction of the DOS for holes from simple optical spectroscopy. This effect is observed for a series of conjugated alternating phenanthrene indenofluorene copolymers [76] and probably more research is needed to confirm such a correlation by involving more copolymer materials.

B. DOS shapes

Another interesting finding of this study is (i) direct observation, using an optical method (TSL), of a pronounced deep exponential tail that follows a Gaussian distribution; and (ii) that this effect turns out to be material dependent—it is seen in CBP and mCBP films, while mCBP-CN, mCP, and mCP-CN host materials feature solely a Gaussian profile with a negligible, if any, exponential tail [cf. Figs. 3(b) and 4(b)]. The origin of such qualitatively different DOS distributions in organic solids deserves more thorough investigation, involving more amorphous organic semiconducting materials, going beyond the scope of the present study. However, a deep exponential tail in disordered organic semiconductors is not a surprising result, but has previously been reported

using different methods. In a series of publications by Van Mensfoort *et al.* [8,72,73], they claimed that their drift-diffusion device model provided a much better description of the experimental temperature-dependent *IV* characteristics measured in some amorphous organic semiconductor (AOS) materials, if one assumes a combination of a Gaussian density of transport states plus superimposed exponential density of trap states. They assume that the charge traps can be responsible for the exponential tail and suggest the following cumulative DOS in realistic organic semiconducting materials [8,72,73]:

$$g(\varepsilon) = \frac{N_t}{\sqrt{2\pi\sigma^2}} \exp\left(-\frac{\varepsilon^2}{2\sigma^2}\right) + \frac{N_{\text{trap}}}{kT_0} \exp\left(\frac{\varepsilon}{kT_0}\right), \quad (7)$$

where σ and N_t are the Gaussian DOS width and the density of transport sites, respectively. T_0 and N_{trap} are the characteristic width of the exponential distribution (for energies $\varepsilon < 0$) and the density of trap sites, respectively. This idea was supported by Hulea *et al.* [17], who scanned the DOS distribution of a poly(*p*-phenylene vinylene) film over a wide energy range using an electrochemically gated transistor and found an almost exponential trap distribution at the deep tail superimposed onto an intrinsic Gaussian DOS distribution. Moreover, several KPFM studies [10,11] provide direct evidence that AOS materials exhibit both a central Gaussian DOS and an exponential tail.

Several theoretical explanations are suggested for the complex DOS distribution observed in AOS. May *et al.* [9] demonstrate that, in a material with molecular dipole moments, exponential tails can develop if negatively or positively charged sites are strongly polarizable. This results in large *induced* dipoles on these charged sites and thereby increases their interaction with the polar environment. Such nonlinear effects of dipolar fields give rise to strong potential fluctuation and thereby lead to the appearance of an exponential tail. Additionally, the same group has recently found that a HOMO level position below 6 eV and LUMO above 3.6 eV, in organic semiconductors, can facilitate hole and electron trapping, respectively [74].

Interestingly, our observations seem to be consistent with the above prediction for a trap-free energy window: virtually no exponential tail is observed for mCP films [cf. Fig. 4(b)], where the HOMO level is at 5.9 eV, i.e., within a "trap-free energy window," inside which organic semiconductors normally do not experience charge trapping [74]. The above concept implies that materials with an ionization energy lower than 6 eV will not exhibit trap-limited hole transport, similarly, an electron affinity above 3.6 eV will not cause electron trapping to limit electron transport [74]. We also find a similar picture in 10-[4-(4,6-diphenyl-1,3,5-triazin-2-yl)phenyl]-9,9-dimethylacridine films featuring no deep exponential tail (not shown here) and where the HOMO level is at 5.8 eV, which is consistent with trap-free conditions. Therefore, we assume that the pure Gaussian distribution observed over a wide energy range might be related to the absence of a significant number of extrinsic traps in this material. On the other hand, mCBP has a HOMO at 6.1 eV, which should facilitate extrinsic charge (hole) trapping, correlated with a very pronounced exponential tail observed by TSL [curve 2 in Fig. 3(b)]. In the case of mCBP-CN and mCP-CN, extrinsic traps are expected, as suggested by consideration of the position of the HOMO-LUMO level. However, we hypothesize that significantly stronger molecular dipole moments in mCBP-CN and mCP-CN might dampen the field variations due to induced dipoles, which give rise predominantly to the Gaussian distribution observed in our experiments [cf. curves 3 and 2 in Figs. 3(b) and 4(b), respectively]. These issues definitely require thorough investigation, which goes beyond the scope of the present study.

Finally, we discuss the implication of the "frequency-to-escape" factor, $\langle S \rangle = 2.7 \times 10^9$ s^{-1}, estimated at the maximum of the TSL peak (cf. Fig. 2). Since both the TSL and the hopping charge-transport process in disordered organic semiconductors are controlled by thermally assisted jumps of relaxed carriers, the mechanisms of which are successfully described in terms of the Miller-Abrahams jump rates [1], it is highly likely that the "frequency-of-escape frequency" has the same meaning in both cases. For disordered semiconductors, it presents the probability of a charge-carrier hop, i.e., tunnels, when energetic resonance occurs. This probability decreases exponentially with the hopping distance, ρ, and is usually described in terms of a homogenous lattice gas (also called the lattice gas model [3]) as

$$\nu = \nu_0 \exp(-2\rho/\rho_0), \quad (8)$$

where ρ_0 is a wave function decay parameter and ν_0 is a frequency factor, which is typically assumed to be equal to the vibrational frequency of about 10^{13} s^{-1}. The lattice gas model is based on the assumption that the hopping distance can be described as $\rho = (M/Ac\delta)^{1/3}$, where M is the molecular weight, A is the Avogadro number, and δ is the sample density. The model ignores the distribution of hopping distances and the distribution of hopping-site energies. Eq. (8) is a key relationship that describes the dependence of charge mobility on the concentration of charge-transporting molecules in molecularly doped polymers [3]. Assuming that the hopping distance, ρ, in mCBP-CN films is equal to the average lattice constant, $a = 11$ Å, as estimated above for this material, and that the estimated TSL frequency-to-escape factor, $\langle S \rangle = 2.7 \times 10^9$ s^{-1}, can be described by the lattice gas model, Eq. (8) yields the wave-function decay parameter, $\rho_0 = 2.68$ Å. This parameter coincides very well with that reported in the literature [3] for conventional charge-transporting molecules, which is typically within a range of 1–2 Å and less often approaches 3 Å. Thus, the relatively

large wave-function decay parameter implies an enhanced intermolecular electronic coupling, which should promote good transport behavior in this material. This is in line with recent simulation results [70] that predict a large average coupling in CBP due to the specific shape of its electronic orbitals, which are uniformly distributed over the periphery of the molecule. This facilitates the overlap of states participating in charge transport and, as a result, leads to a fairly large mobility prefactor of $\mu_0 = 0.8\ \mathrm{cm^2V^{-1}s^{-1}}$ in this material.

V. CONCLUSIONS

We demonstrate that the DOS distribution in neat OLED host materials can be well determined by the low-temperature fractional TSL technique. This is proven by comparison of the TSL results with DOS parameters obtained by computer simulations, as carried out in the present study, and from available charge-transport measurements. We perform comparative TSL studies of two series of OLED host materials possessing different polarities: (i) CBP, mCBP, and mCBP-CN; and (ii) mCP and mCP-CN. Their dipole moments vary from almost zero for nonpolar CBP to 6 D in strongly polar mCP-CN. We find that the DOS distribution broadens significantly with increasing molecular dipole moments, which can be well described by the dipolar-disorder model, but only for materials belonging to the same series of derivatives that possess similar polarizability of cations and neutral molecules. We find that the DOS widths of these two series of materials are offset by a constant amount, with a broader DOS for CP derivatives, compared with CBP-based compounds at equivalent polarity. This is confirmed by simulations that demonstrate a similar trend in the variation of DOS. Larger energetic disorder in CP derivatives is attributed to smaller polarizability of both their neutral and cation states. Therefore, the electrostatic disorder of CP derivatives is not screened by induction as much as the disorder of CBP derivatives. Additionally, the significant nonpolar component of the disorder observed in CP derivatives is consistent with the theoretical prediction. The dipolar energy-disorder component of the DOS, as extracted from the TSL experiment, demonstrates a similar increase with the magnitude of the molecular dipole moment for all materials considered in this work, implying that the dipolar-disorder model is applicable to such OLED host materials. Such behavior is expected if the intersite distance is similar in these systems. Finally, we find that a deep exponential tail accompanies a Gaussian distribution in CBP and mCBP films. The origin of this effect will be the subject of further investigation by the authors.

ACKNOWLEDGMENTS

The authors acknowledge funding through the EU Marie Skłodowska-Curie ITN TADF*life* grant (Grant No. 812872). This research is also supported by the European Research Council under ERC Grant No. 835133 (ULTRALUX), VW Foundation, and by the National Academy of Science of Ukraine (Project No. VC/205) and NRFU Grant No. 2020.01/0144. The authors thank Rama Dhali from the University of Parma for calculation of the dipole moments of the materials studied in this paper. D.A. thanks the BMBF for an InterPhase grant (Grant No. FKZ 13N13661) and the European Union Horizon 2020 research and innovation program "Widening materials models" under Grant No. 646259 (MOSTOPHOS). This research is supported by the King Abdullah University of Science and Technology (KAUST), via the Competitive Research Grants (CRG) Program. D.A. acknowledges KAUST for hosting his sabbatical.

[1] H. Bässler, Charge transport in disordered organic photoconductors a monte carlo simulation study, Phys. Status Solidi B **175**, 15 (1993).

[2] A. Köhler and H. Bässler, *Electronic Processes in Organic Semiconductors: An Introduction* (John Wiley & Sons, Weinheim, 2015).

[3] P. M. Borsenberger and D. Weiss, *Organic Photoreceptors for Xerography* (CRC Press, New York, 1998).

[4] S. D. Baranovskii, Mott lecture: Description of charge transport in disordered organic semiconductors: Analytical theories and computer simulations, Phys. Status Solidi A **215**, 1700676 (2018).

[5] J. Oelerich, D. Huemmer, and S. Baranovskii, How to Find out the Density of States in Disordered Organic Semiconductors, Phys. Rev. Lett. **108**, 226403 (2012).

[6] S. V. Novikov, Far tails of the density of states in amorphous organic semiconductors, J. Chem. Phys. **143**, 164510 (2015).

[7] V. Arkhipov, P. Heremans, E. Emelianova, and H. Baessler, Effect of doping on the density-of-states distribution and carrier hopping in disordered organic semiconductors, Phys. Rev. B **71**, 045214 (2005).

[8] S. Van Mensfoort, J. Billen, S. Vulto, R. Janssen, and R. Coehoorn, Electron transport in polyfluorene-based sandwich-type devices: Quantitative analysis of the effects of disorder and electron traps, Phys. Rev. B **80**, 033202 (2009).

[9] F. May, B. Baumeier, C. Lennartz, and D. Andrienko, Can Lattice Models Predict the Density of States of Amorphous Organic Semiconductors?, Phys. Rev. Lett. **109**, 136401 (2012).

[10] O. Tal, Y. Rosenwaks, Y. Preezant, N. Tessler, C. Chan, and A. Kahn, Direct Determination of the Hole Density of States in Undoped and Doped Amorphous Organic Films with High Lateral Resolution, Phys. Rev. Lett. **95**, 256405 (2005).

[11] K. Celebi, P. Jadhav, K. Milaninia, M. Bora, and M. Baldo, The density of states in thin film copper phthalocyanine measured by kelvin probe force microscopy, Appl. Phys. Lett. **93**, 317 (2008).

[12] M. Pope and C. E. Swenberg, Electronic processes in organic solids, Annu. Rev. Phys. Chem. **35**, 613 (1984).

[13] H. Bässler, in *Disorder Effect on Relaxational Processes*, edited by Richert R., Blumen A. (Springe-Verlagr, Berlin Heidelberg New York, 1994), pp. 485–507.

[14] F. Schauer, S. Nešpůrek, and H. Valerián, Temperature dependent space-charge-limited currents in amorphous and disordered semiconductors, J. Appl. Phys. **80**, 880 (1996).

[15] S. Olthof, S. Mehraeen, S. K. Mohapatra, S. Barlow, V. Coropceanu, J.-L. Brédas, S. R. Marder, and A. Kahn, Ultralow Doping in Organic Semiconductors: Evidence of Trap Filling, Phys. Rev. Lett. **109**, 176601 (2012).

[16] V. Y. Aristov, O. Molodtsova, V. Maslyuk, D. Vyalikh, V. Zhilin, Y. A. Ossipyan, T. Bredow, I. Mertig, and M. Knupfer, Electronic structure of pristine CuPc: Experiment and calculations, Appl. Surf. Sci. **254**, 20 (2007).

[17] I. Hulea, H. Brom, A. Houtepen, D. Vanmaekelbergh, J. Kelly, and E. Meulenkamp, Wide Energy-Window View on the Density of States and Hole Mobility in Poly (p-Phenylene Vinylene), Phys. Rev. Lett. **93**, 166601 (2004).

[18] A. Kadashchuk, Y. Skryshevskii, A. Vakhnin, N. Ostapenko, V. Arkhipov, E. Emelianova, and H. Bässler, Thermally stimulated photoluminescence in disordered organic materials, Phys. Rev. B **63**, 115205 (2001).

[19] V. Arkhipov, E. Emelianova, A. Kadashchuk, and H. Bässler, Hopping model of thermally stimulated photoluminescence in disordered organic materials, Chem. Phys. **266**, 97 (2001).

[20] A. Kadashchuk, A. Vakhnin, Y. Skryshevski, V. Arkhipov, E. Emelianova, and H. Bässler, Thermally stimulated luminescence in π-conjugated polymers containing fluorene and spirobifluorene units, Chem. Phys. **291**, 243 (2003).

[21] A. Kadashchuk, N. Ostapenko, V. Zaika, and S. Nešpurek, Low-temperature thermoluminescence in poly (methylphenylsilylene), Chem. Phys. **234**, 285 (1998).

[22] A. Kadashchuk, Y. Skryshevski, Y. Piryatinski, A. Vakhnin, E. Emelianova, V. Arkhipov, H. Bässler, and J. Shinar, Thermally stimulated photoluminescence in poly (2, 5-dioctoxy p-phenylene vinylene), J. Appl. Phys. **91**, 5016 (2002).

[23] S. A. Patil, U. Scherf, and A. Kadashchuk, New conjugated ladder polymer containing carbazole moieties, Adv. Funct. Mater. **13**, 609 (2003).

[24] A. Kadashchuk, S. Schols, A. Vakhnin, J. Genoe, and P. Heremans, Triplet dynamics and charge carrier trapping in triplet-emitter doped conjugated polymers, Chem. Phys. **358**, 147 (2009).

[25] A. Kadashchuk, V. I. Arkhipov, C.-H. Kim, J. Shinar, D.-W. Lee, Y.-R. Hong, J.-I. Jin, P. Heremans, and H. Bässler, Localized trions in conjugated polymers, Phys. Rev. B **76**, 235205 (2007).

[26] I. Fishchuk, A. Kadashchuk, A. Vakhnin, Y. Korosko, H. Bässler, B. Souharce, and U. Scherf, Transition from trap-controlled to trap-to-trap hopping transport in disordered organic semiconductors, Phys. Rev. B **73**, 115210 (2006).

[27] A. Kadashchuk, D. Weiss, P. Borsenberger, S. Nešpurek, N. Ostapenko, and V. Zaika, The origin of thermally stimulated luminescence in neat and molecularly doped charge transport polymer systems, Chem. Phys. **247**, 307 (1999).

[28] A. Kadashchuk, D. Weiss, P. Borsenberger, N. Ostapenko, V. Zaika, and Y. Skryshevski, Effect of extrinsic traps on thermally stimulated luminescence in molecularly doped polymers, Synth. Met. **109**, 177 (2000).

[29] P. V. Soroka, A. Y. Vakhnin, Y. A. Skryshevskiy, O. P. Boiko, M. I. Anisimov, Y. L. Slominskiy, V. G. Nazarenko, J. Genoe, and A. Kadashchuk, Charge carrier trapping in highly-ordered lyotropic chromonic liquid crystal films based on ionic perylene diimide derivatives, Eur. Phys. J.: Appl. Phys. **68**, 30201 (2014).

[30] A. Fakharuddin, W. Qiu, G. Croes, A. Devižis, R. Gegevičius, A. Vakhnin, C. Rolin, J. Genoe, R. Gehlhaar, A. Kadashchuk, V. Gulbinas, and P. Heremans, Reduced efficiency roll-Off and improved stability of mixed 2D/3D perovskite light emitting diodes by balancing charge injection, Adv. Funct. Mater. **29**, 1904101 (2019).

[31] I. Tale, Trap spectroscopy by the fractional glow technique, Phys. Status Solidi A **66**, 65 (1981).

[32] H. Gobrecht and D. Hofmann, Spectroscopy of traps by fractional glow technique, J. Phys. Chem. Solids **27**, 509 (1966).

[33] Y. Gorohovatsky and H. Bordovsky, *Thermally Activational Current Spectroscopy of High-Resistance Semiconductors and Dielectrics* (Izd. Nauka, Moscow, 1991).

[34] W. L. Jorgensen and J. Tirado-Rives, Potential energy functions for atomic-level simulations of water and organic and biomolecular systems, Proc. Natl. Acad. Sci. **102**, 6665 (2005).

[35] W. L. Jorgensen and J. Tirado-Rives, The OPLS [optimized potentials for liquid simulations] potential functions for proteins, energy minimizations for crystals of cyclic peptides and crambin, J. Am. Chem. Soc. **110**, 1657 (1988).

[36] W. L. Jorgensen, D. S. Maxwell, and J. Tirado-Rives, Development and testing of the OPLS all-atom force field on conformational energetics and properties of organic liquids, J. Am. Chem. Soc. **118**, 11225 (1996).

[37] C. M. Breneman and K. B. Wiberg, Determining atom-centered monopoles from molecular electrostatic potentials. The need for high sampling density in formamide conformational analysis, J. Comput. Chem. **11**, 361 (1990).

[38] C. Poelking, E. Cho, A. Malafeev, V. Ivanov, K. Kremer, C. Risko, J.-L. Brédas, and D. Andrienko, Characterization of charge-carrier transport in semicrystalline polymers: Electronic couplings, site energies, and charge-carrier dynamics in poly (bithiophene-alt-thienothiophene)[PBTTT], J. Phys. Chem. C **117**, 1633 (2013).

[39] G. Bussi, D. Donadio, and M. Parrinello, Canonical sampling through velocity rescaling, J. Chem. Phys. **126**, 014101 (2007).

[40] H. J. Berendsen, J. v. Postma, W. F. van Gunsteren, A. DiNola, and J. R. Haak, Molecular dynamics with coupling to an external bath, J. Chem. Phys. **81**, 3684 (1984).

[41] B. Hess, C. Kutzner, D. Van Der Spoel, and E. Lindahl, GROMACS 4: Algorithms for highly efficient, load-balanced, and scalable molecular simulation, J. Chem. Theory Comput. **4**, 435 (2008).

[42] S. Pronk, S. Páll, R. Schulz, P. Larsson, P. Bjelkmar, R. Apostolov, M. R. Shirts, J. C. Smith, P. M. Kasson, D. van der Spoel, B. Hess, and E. Lindahl, GROMACS 4.5: A high-throughput and highly parallel open source molecular simulation toolkit, Bioinformatics **29**, 845 (2013).

[43] A. Stone, *The Theory of Intermolecular Forces* (Clarendon Press, Oxford, 1997).

[44] G. D'Avino, L. Muccioli, F. Castet, C. Poelking, D. Andrienko, Z. G. Soos, J. Cornil, and D. Beljonne, Electrostatic phenomena in organic semiconductors: Fundamentals and implications for photovoltaics, J. Phys.: Condens. Matter. **28**, 433002 (2016).

[45] C. Poelking and D. Andrienko, Long-range embedding of molecular ions and excitations in a polarizable molecular environment, J. Chem. Theory Comput. **12**, 4516 (2016).

[46] B. T. Thole, Molecular polarizabilities calculated with a modified dipole interaction, Chem. Phys. **59**, 341 (1981).

[47] P. T. Van Duijnen and M. Swart, Molecular and atomic polarizabilities: Thole's model revisited, J. Phys. Chem. A **102**, 2399 (1998).

[48] A. J. Stone, Distributed multipole analysis: Stability for large basis sets, J. Chem. Theory Comput. **1**, 1128 (2005).

[49] V. Rühle, A. Lukyanov, F. May, M. Schrader, T. Vehoff, J. Kirkpatrick, B. R. Baumeier, and D. Andrienko, Microscopic simulations of charge transport in disordered organic semiconductors, J. Chem. Theory Comput. **7**, 3335 (2011).

[50] E. W. Forsythe, D. C. Morton, C. W. Tang, and Y. Gao, Trap states of tris-8-(hydroxyquinoline) aluminum and naphthyl-substituted benzidine derivative using thermally stimulated luminescence, Appl. Phys. Lett. **73**, 1457 (1998).

[51] J. Simmons and G. Taylor, High-field isothermal currents and thermally stimulated currents in insulators having discrete trapping levels, Phys. Rev. B **5**, 1619 (1972).

[52] G. G. Malliaras, Y. Shen, D. H. Dunlap, H. Murata, and Z. H. Kafafi, Nondispersive electron transport in Alq 3, Appl. Phys. Lett. **79**, 2582 (2001).

[53] H. Bässler, Localized states and electronic transport in single component organic solids with diagonal disorder, Phys. Stat. Sol. B **107**, 9 (1981).

[54] R. Eiermann, W. Hofberger, and H. Bässler, Localized valence states in the forbidden gap of non-crystalline tetracene, J. Non·Cryst. Solids **28**, 415 (1978).

[55] B. Movaghar, B. Ries, and M. Grünewald, Diffusion and relaxation of energy in disordered systems: Departure from mean-field theories, Phys. Rev. B **34**, 5574 (1986).

[56] M. Era, K. Mori, and N. Mototsu, Analysis of hole mobility of fluorene derivative films based on the disorder model and relationship between disorder free mobility and reorganization energy in the marcus theory. In *Organic Light Emitting Materials and Devices XVII*, edited by F. So and C. Adachi (International Society for Optics and Photonics, 2013), Vol. 8829, p. 88290N.

[57] S. Athanasopoulos, S. T. Hoffmann, H. Bässler, A. Köhler, and D. Beljonne, To hop or not to hop? understanding the temperature dependence of spectral diffusion in organic semiconductors, J. Phys. Chem. Lett. **4**, 1694 (2013).

[58] A. Dieckmann, H. Bässler, and P. Borsenberger, An assessment of the role of dipoles on the density-of-states function of disordered molecular solids, J. Chem. Phys. **99**, 8136 (1993).

[59] P. Borsenberger and H. Bässler, Concerning the role of dipolar disorder on charge transport in molecularly doped polymers, J. Chem. Phys. **95**, 5327 (1991).

[60] P. Borsenberger, *Electrical and Related Properties of Organic Solids* (Springer, Dordrecht, 1997), pp. 25.

[61] S. Novikov and A. Vannikov, *Hopping charge transport in disordered organic materials: Where is the disorder?*, J. Phys. Chem. C **113**, 2532 (2009).

[62] R. H. Young, Dipolar lattice model of disorder in random media analytical evaluation of the Gaussian disorder model, Philos. Mag. B **72**, 435 (1995).

[63] C. Madigan and V. Bulović, Charge Carrier Energy Disorder in Polar Amorphous Organic Thin Films, Phys. Rev. Lett. **97**, 216402 (2006).

[64] P. Borsenberger, M. Detty, and E. Magin, Electron transport in vapor deposited molecular glasses, Phys. Stat. Sol. B **185**, 465 (1994).

[65] P. M. Borsenberger and J. J. Fitzgerald, Effects of the dipole moment on charge transport in disordered molecular solids, J. Phys. Chem. **97**, 4815 (1993).

[66] V. Mimaite, J. V. Grazulevicius, R. Laurinaviciute, D. Volyniuk, V. Jankauskas, and G. Sini, Can hydrogen bonds improve the hole-mobility in amorphous organic semiconductors? experimental and theoretical insights, J. Mater. Chem. C **3**, 11660 (2015).

[67] P. Borsenberger, E. Magin, M. O'regan, and J. Sinicropi, The role of dipole moments on hole transport in triphenylamine-doped polymers, J. Polym. Sci., Part B: Polym. Phys. **34**, 317 (1996).

[68] P. Borsenberger and M. O'Regan, The role of dipole moments on hole transport in triphenylamine doped poly (styrene), Chem. Phys. **200**, 257 (1995).

[69] R. H. Young and J. J. Fitzgerald, Effect of polar additives on charge transport in a molecularly doped polymer: Survey of various additives, J. Chem. Phys **102**, 2209 (1995).

[70] N. B. Kotadiya, A. Mondal, S. Xiong, P. W. Blom, D. Andrienko, and G. J. A. Wetzelaer, Rigorous characterization and predictive modeling of hole transport in amorphous organic semiconductors, Adv. Electron. Mater. **4**, 1800366 (2018).

[71] P. K. Nayak and N. Periasamy, Calculation of ionization potential of amorphous organic thin-films using solvation model and DFT, Org. Electron. **10**, 532 (2009).

[72] S. Van Mensfoort, R. De Vries, V. Shabro, H. Loebl, R. Janssen, and R. Coehoorn, Electron transport in the organic small-molecule material BAlq—the role of correlated disorder and traps, Org. Electron. **11**, 1408 (2010).

[73] S. Van Mensfoort and R. Coehoorn, Effect of Gaussian disorder on the voltage dependence of the current density in sandwich-type devices based on organic semiconductors, Phys. Rev. B **78**, 085207 (2008).

[74] N. B. Kotadiya, A. Mondal, P. W. Blom, D. Andrienko, and G.-J. A. Wetzelaer, A window to trap-free charge transport in organic semiconducting thin films, Nat. Mater. **18**, 1182 (2019).

[75] A. Mondal, L. Paterson, J. Cho, K.-H. Lin, B. van der Zee, G. Wetzelaer, A. Stankevych, A. Vakhnin, J. Kim, A. Kadashchuk, P. W. M. Blom, F. May, and D. Andrienko, Physical Properties of OLED Host Materials (submitted to Chemical Physics Review, 2021).

[76] S. T. Hoffmann, F. Jaiser, A. Hayer, H. Bässler, T. Unger, S. Athanasopoulos, D. Neher, and A. Köhler, How do disorder, reorganization, and localization influence the hole mobility in conjugated copolymers?, J. Am. Chem. Soc. **135**, 1772 (2013).

[77] http://www.iop.kiev.ua/~cryo/index_en.php.

[78] https://gaussian.com/polar/.